Title
Optic nerve head and intraocular pressure in the guinea pig eye

Authors
Ostrin, Lisa A
Wildsoet, Christine F

Publication Date
2016-05-01

DOI
10.1016/j.exer.2015.12.007

Peer reviewed

HHS Public Access

Author manuscript

Exp Eye Res. Author manuscript; available in PMC 2017 May 01.

Published in final edited form as:

Exp Eye Res. 2016 May ; 146: 7–16. doi:10.1016/j.exer.2015.12.007.

Optic Nerve Head and Intraocular Pressure in the Guinea Pig Eye

Lisa A Ostrin[a] and **Christine F Wildsoet**[b]

[a]College of Optometry University of Houston, 4901 Calhoun, Houston, TX 77004, USA

[b] School of Optometry University of California Berkeley, 588 Minor Hall, Berkeley, CA 94720, USA, wildsoet@berkeley.edu

Abstract

The guinea pig is becoming an increasingly popular model for studying human myopia, which carries an increased risk of glaucoma. As a step towards understanding this association, this study sought to characterize the normal, developmental intraocular pressure (IOP) profiles, as well as the anatomy of the optic nerve head (ONH) and adjacent sclera of young guinea pigs. IOP was tracked in pigmented guinea pigs up to 3 months of age. One guinea pig was imaged *in vivo* with OCT and one with a fundus camera. The eyes of pigmented and albino guinea pigs (ages 2 months) were enucleated and sections from the posterior segment, including the ONH and surrounding sclera, processed for histological analyses - either hematoxylin and eosin (H&E) staining of paraffin embedded, sectioned tissue (n = 1), or cryostat sectioned tissue, processed for immunohistochemistry (n = 3), using primary antibodies against collagen types I-V, elastin, fibronectin and glial fibrillary acidic protein (GFAP). Transmission and scanning electron microscopy (TEM, SEM) studies of ONHs were also undertaken (n = 2 & 5 respectively). Mean IOPs ranged from 17.33 to 22.7 mmHg , increasing slightly across the age range studied, and the IOPs of individual animals also exhibited diurnal variations, peaking in the early morning (mean of 25.8, mmHg, ~9 am), and decreasing across the day. H&E-stained sections showed retinal ganglion cell axons organized into fascicles in the prelaminar and laminar region of the ONHs, with immunostained sections revealing collagen types I, III, IV and V, as well as elastin, GFAP and fibronectin in the ONHs. SEM revealed a well-defined lamina cribrosa (LC), with radially-oriented collagen beams. TEM revealed collagen fibrils surrounding non-myelinated nerve fiber bundles in the LC region, with myelination and decreased collagen posterior to the LC. The adjacent sclera comprised mainly crimped collagen fibers in a crisscross arrangement. Both the sclera and LC were qualitatively similar in structure in pigmented and albino guinea pigs. The well-organized, collagen-based LC of the guinea pig ONH is similar to that described for tree shrews and more similar to the human LC than that of other rodents that lack collagen. Based on these latter structural similarities the guinea pig would seem a promising model for investigating the relationship between myopia and glaucoma.

corresponding author ; Email: lostrin@central.uh.edu

Keywords

myopia; glaucoma; optic nerve head; lamina cribrosa; guinea pig; intraocular pressure

1. Introduction

The guinea pig has become a popular model for the study of human myopia (Howlett and McFadden, 2006, 2009), which is now epidemic in some populations (Vitale et al., 2009). Myopia, or nearsightedness, refers to the condition in which light rays from distant objects come to focus in front of the retina, resulting in blurred retinal images when this focusing error is not corrected. In most cases, the mismatch between the eye's length and its refracting power is a result of the eye being longer than normal. Importantly, the risks of potentially blinding pathological complications, including retinal detachment, macular degeneration and primary open angle glaucoma (POAG) are closely associated with the amount of myopia (Casson et al., 2007; Jonas and Budde, 2005; Liang et al.; Xu et al., 2007b). As the prevalence of high myopia, commonly defined as greater than −6 D, has also risen along with myopia prevalence overall, high myopia is expected to result in a higher number of associated pathologies (Pan et al., 2013; Pierro et al., 1992). In addition, uncorrected myopia is a leading cause of functional blindness (Pascolini and Mariotti, 2012).

In relation to POAG, a number of studies have reported increased risks for myopes, by two- to three-fold, with high myopes being more at risk (Jonas and Budde, 2005; Mitchell et al., 1999). In the Beaver Dam study, it was found that compared to emmetropes, myopes recorded higher IOPs and were also 60% more likely to have POAG (Wong et al., 2003). While glaucoma appears to be a multi-factorial ocular disease, damage to the retinal ganglion cells (RGCs) and vision loss represent unifying end-points. Also of note in two recent studies, glaucomatous visual field damage and progression were found to be worse with increasing myopia (Perdicchi et al., 2007); optic nerve fiber loss was also more pronounced in highly myopic eyes than in less myopic eyes, implying greater susceptibility for optic nerve fiber damage in more myopic eyes, which also had larger optic discs (Jonas and Budde, 2005). Some of the evidence linking myopia with glaucoma and other sight-threatening pathologies is summarized in a recent review by Flitcroft (Flitcroft, 2012). However, note that some studies have reported no relationship between myopia and glaucoma progression in normal tension glaucoma (Sohn et al., 2010) and POAG (Hung et al., 2015).

In relation to nerve fiber loss in glaucoma, much attention has been paid to the lamina cribrosa (LC), which, in the human eye, is comprised of a collagenous meshwork spanning the scleral canal, deep in the optic nerve head, through which RGC axons pass to form the optic nerve. Changes in its structure have been strongly implicated in glaucomatous damage (Burgoyne et al., 2005; Quigley et al., 1983). Specifically, in glaucoma the LC is reported to deform, with the entire structure bowing posteriorly and its components compressed (Quigley et al., 1983; Yang et al., 2007). The deformation of the LC is postulated to generate shearing forces that disrupt critical transport processes within the axons of RGCs (Quigley et al., 1979; Sossi and Anderson, 1983). Other possible etiologies of axonal damage include

impaired blood flow (Hayreh, 1969), laminar microarchitecture remodeling (Roberts et al., 2009), and biochemical alterations in extracellular matrix (Morrison et al., 1990). When IOP is artificially increased, the LC undergoes an anterior-posterior deformation, along with scleral canal expansion (Sigal et al., 2011), consistent with the suggestion that the biomechanical properties of the peripapillary sclera play an important role in the ONH changes in glaucoma (Girard et al., 2009a). Other glaucoma-related structural changes in the LC, specifically, increases in the area of laminar pores as well as shape changes (elongation) of the LC pores, have been observed in monkey eyes using advanced *in vivo* adaptive optics imaging (Vilupuru et al., 2007).

Of relevance to the current study, a previous study of enucleated highly myopic human eyes with and without glaucoma revealed the LCs of highly myopic eyes to be significantly thinner compared to those of less myopic eyes, and even thinner in highly myopic eyes with glaucoma (Jonas et al., 2004). The LCs of myopic eyes have also been reported to be more have more anterior surface irregularities (Miki et al., 2015). Either or both of these differences could contribute to the apparently greater susceptibility of myopes to glaucomatous optic disc changes (Fong et al., 1990; Scott and Grosvenor, 1993).

Of animal models used to study myopia, the chicken is one of the most widely used (Troilo et al., 1987; Wallman et al., 1987), yet it lacks a collagenous LC, and also lacks a concentration of astrocytic filaments in the retinal optic nerve junction (Morcos and Chan-Ling, 2000). Of animals currently being used for glaucoma research, well-organized collagenous LCs are present in the pig (Brooks et al., 1998), cat (Radius and Bade, 1982), dog (Brooks et al., 1989), and monkey (Gaasterland and Kupfer, 1974), but only one, the monkey, is also used as a myopia model.

While rodent models have been developed for many ocular diseases, including myopia and glaucoma (Faulkner et al., 2007; Gross et al., 2003), it is of interest that two of them, the mouse and rat, have non-collagenous LCs (Table 1)(Johansson, 1987; May and Lutjen-Drecoll, 2002). Astrocytes and oligodendrocytes represent the main non-neuronal, support component of the optic nerve head of rats and mice (Morcos and Chan-Ling, 2000). In a comprehensive study of OHN structures involving 18 different rodent species (Rodriguez-Ramos Fernandez and Dubielzig, 2013), the presence of an LC was confirmed in 4 species, including porcupine, capybara, flying squirrel and western gray squirrel, while the Norway rat and three species of mice were found to lack a LC. The lack of relevant histological sections of the optic nerve precluded evaluation of the LC for several species, including the guinea pig, which along with the mouse, also has application in myopia research. Nonetheless, several other studies have suggested that the guinea pig does have a LC, although its structure has not been studied in detail (Fujita et al., 2000; Furuta et al., 1993; Johansson, 1987). The study described here aimed to correct this deficiency – using a variety of microscopy techniques to fully characterize the ONH and adjacent sclera of nonmyopic guinea pig eyes, as well as to establish developmental intraocular pressure (IOP) profiles for the same.

2. Methods and Methods

2.1 Animals

Pigmented and albino guinea pigs were obtained from Elm Hill Labs (MA, USA). Albino animals were included because of their availability, reports of refractive error abnormalities (Jiang et al., 2014; Wang et al., 2007), and use in other ocular studies (Pucker et al., 2014). Animals were maintained on a 12-hour light/dark cycle and provided food and water ad libitum. For *in vivo* imaging, animals were anesthetized with ketamine (30 mg/ml) and xylazine (3 mg/ml). For *in vitro* studies of ocular tissue, animals were euthanized with an intracardial injection of sodium pentobarbital and eyes then enucleated and processed as described in detail below. The procedures used and numbers of animals used in each case are summarized in Table 2. Protocols were approved by the UC Berkeley and University of Houston Animal Care and Use Committees and conformed to the ARVO statement for the Use of Animals in Ophthalmic and Vision Research.

2.2 Intraocular pressure measurements

Pigmented guinea pigs (n=6) underwent intraocular pressure (IOP) measurements on a weekly basis from ages 2 to 7 weeks, then monthly up to 3 months of age. Measurements were always taken at the same time of day (afternoon), to avoid any confounding effect of diurnal rhythms. Guinea pigs were awake and handheld for measurement, which made use of a rebound tonometer, following manufacturer instructions and set to the rat calibration (TonoLab, Colonial Medical Supply, NH, USA). At each time point, three sets of six measurements were recorded on the right and left eyes, and averaged for each eye.

Diurnal IOP rhythms were evaluated in 12 adult pigmented guinea pigs (age 12-18 months). Using a rebound tonometer as described above, IOPs were recorded from their right eyes at two-hour intervals across a 24-hour period. Ten measurements were recorded at each time point and averaged. During the dark phase when lights were off (7:00 pm – 7:00 am), measurements were made in the dark using a dim red LED headlamp.

2.3 *In vivo* imaging

One 4 month-old pigmented guinea pig underwent *in vivo* fundus imaging. After pupil dilation with 2.5% phenylephrine and 1% tropicamide, fundus images were captured with a Visucam Pro NM fundus camera (Zeiss, Dublin, CA). Another 2 month-old pigmented guinea pig was imaged *in vivo* with spectral domain optical coherence tomography (SD-OCT, Bioptigen, NC, USA), which uses a wavelength of 840 nm, and a scan rate of approximately 32,000 A-scans per second, yielding a resolution better than 3 μm. Scan parameters included a 14 mm × 14 mm rectangle with 1000 A-scans per B-scan, 100 B-scans, and 3 B-scans per frame. For imaging, the guinea pig was anesthetized and positioned on a custom-built stage. A speculum was inserted in the eye to be imaged; the eye was then aligned with the optics of the instrument, the position of the reference arm adjusted appropriately to obtain a flat B-scan, a fundus image captured, and the retina then scanned using a custom rectangular volume protocol centered over the optic nerve head. Images were registered and averaged off-line.

2.4 Histology, Immunohistochemistry and Ultrastructure

Four different techniques were applied to characterize the optic nerve head architecture – standard histology with hematoxylin and eosin (H&E) staining applied to paraffin-embedded sections (n=1 pigmented eye), immunohistochemistry applied to cryostat sections (n=3 pigmented eyes), transmission electron microscopy (TEM; n=1 pigmented eye, n= 1 albino eye), and scanning electron microscopy (SEM; n=2 pigmented eyes, n= 3 albino eyes).

For H&E staining, one eye of a pigmented euthanized guinea pig was enucleated and fixed overnight in 4% paraformaldehyde. The eye then underwent dehydration and paraffin infiltration. Following sectioning, the slides were de-paraffinized with xylene and hydrated. The slides were stained with hematoxylin, rinsed, and stained with eosin. After a final dehydration, slides were mounted with coverslips and imaged.

For immunohistochemistry, the eyes of three euthanized pigmented guinea pigs (aged 2 months) were enucleated and fixed overnight at 4°C in a solution of 4% paraformaldehyde and 3% sucrose, then cryoprotected in 20% sucrose at 4°C for 6 h, before being embedded in a 1:1 solution of OCT and 20% sucrose and snap frozen with liquid nitrogen. Eight μm cryostat sections were cut from the posterior segment of the eye, which included the ONH. Sections including the proximal optic nerve were stained with primary antibodies for collagen types I-V, elastin, fibronectin and glial fibrillary acidic protein (GFAP), selected on the basis of the known composition of human, non-human primate, and tree shrew ONHs. After incubation in primary antibodies, the sections were then incubated in appropriate secondary AlexaFluor 488 antibodies. Images were captured using a DeltaVision Spectris deconvolution microscope (Applied Precision, Issequah, WA), as z-stacks through appropriate filters for DAPI and FITC fluorescence. Z-stacks were later deconvolved and shown as projections. As a control for nonspecific muscarinic staining, additional sections were prepared by omitting the primary antibody, then incubating the sections in the secondary antibody.

2.5 Optic nerve head ultrastructure

For both transmission and scanning electron microscopy (TEM and SEM, respectively), the optic nerve and surrounding 2 mm ring of sclera was collected from individual eyes and fixed with 2% gluteraldehyde. For TEM, the tissue underwent a 1% osmium tetroxide fixation followed by dehydration. Samples were then embedded in resin using a vacuum microwave infiltration method. Ultrathin sections were cut with a diamond knife and placed on grids. Samples were viewed using TEM (FEI Tecnai 12).

For SEM, the tissue then underwent alkali maceration with 10% NaOH for 48-76 h to remove cellular components, was rinsed and stained with 1% osmium tetroxide for 2 h, and then dehydrated through a graded ethanol series and critical point drying. Samples were mounted on aluminum stubs and imaged with an SEM (Hitachi TM-1000, Japan). Images were analyzed off-line with ImageJ (NIH, MD, USA), to determine maximum and minimum diameters and areas.

3. Results

3.1 Intraocular pressure

IOP data for right and left eyes are presented in Figure 1a. Values for the two eyes of individual animals were similar ($p>0.05$). Across the age range studied here, 2 weeks to 3 months, IOPs showed an early small increase and thereafter appeared to stabilize. This pattern is reflected in the following mean values of 17.6 ± 2.65 mmHg (mean ± SD) at 2 weeks of age and 22.7 ± 2.3 mmHg at 3 months of age. The means for individual eyes of individual animals ranged over the course of the 3-month study period from 17.3 to 25.7 mmHg.

Diurnal IOP data for right eyes of adults are shown in Figure 1b. The highest average IOP of 25.8 ± 2.5 mmHg (mean ± SE), was recorded at 9:00 am, with IOP thereafter decreasing across the day to a minimum at 9:00 pm of 20.1 ± 0.9 mmHg.

3.2 In vivo imaging of ocular fundus & ONH

A representative normal fundus picture from a 4 months-old pigmented guinea pig is shown in Figure 2. The retina is largely avascular, allowing an uninterrupted view of the nerve fiber striations radiating from the optic nerve head (disc). In this example, the camera was focused on the nerve fiber layer, rendering the optic disc rim and cup slightly out-of-focus. The optic disc has distinct margins and a barely visible cup, with a network of fine blood vessels, which in this case, did not extend onto the neural retina.

Representative images captured using the Bioptogen SD-OCT instrument from another younger (2 months-old) pigmented guinea pig are shown in Figure 3. The low resolution, fundus image (Figure 3a) shows the optic nerve head and surrounding avascular retina, while the cross-sectional OCT image shows the various retinal layers, including the nerve fiber layer, which are readily visible, as is the retina-optic disc boundary, where Bruch's membrane terminates. The fine structural organization of the optic nerve cannot be resolved but were subsequently characterized from fixed tissue samples.

3.3 Histology & Immunostaining of ONH & adjacent Sclera

Nerve fibers traverse through the scleral opening to form the optic nerve, which expands in diameter after exiting the globe. The organization of retinal ganglion cell axons into fascicles begins in the prelaminar region, becoming more clearly defined in the laminar region, as evident in the H & E-stained sections of the ONH (Figure 4). Immunostained sections of the optic nerve head confirmed the presence collagen types I, III, IV and V, as well as elastin, GFAP and fibronectin in the structural elements of the ONH (Figure 5). Collagen also predominates in the fibrous sclera, which lies external to the choroid and is continuous with the dura mater surrounding the optic nerve.

3.4 Ultrastructure of ONH

TEM images of the guinea pig ONH revealed many parallels with the organization of the human ONH. In the prelaminar LC region, there are bundles of non-myelinated nerve fibers (retinal ganglion cell axons), surrounded by collagen fibrils (Figures 6A, D), while in the

post-laminar region, the nerve axons are myelinated (Figures 6B, E). In the adjacent sclera, densely packed collagen fibrils are arranged in a criss-cross pattern. Images from the eyes of albino and pigmented animals were qualitatively similar in all respects.

SEM images of digested ONH preparations provided additional insight into the structural organization of the ONH, revealing a well-defined, multilayered lamina cribrosa, with radially-oriented bundles of connective tissue, including collagen beams (Figure 7). The central aggregation of collagen corresponds to the location of blood vessels visible in fundus images (Figure 2b), and presumably representing supporting collagenous sheaths. The scleral canals (openings) are elliptical in shape, with average dimensions of the longest and shortest axes of 352.4 ± 57.41 μm and 285.4 ± 34 μm respectively, corresponding to an average scleral canal area of 3.15×10^5 μm^2. The orientation of the long and short axes of the ONH in the intact eye is not known, the nature of tissue processing precluding orientation markers being applied and retained in dissected optic nerve specimens. Here also there were no qualitative or quantitative differences between measurements obtained from pigmented and albino animals.

4. Discussion

This study, which was largely focused on the structure of the optic nerve head in the guinea pig, found it to share many similarities in structure and biochemical composition to that of higher order mammals, non-human primates and humans. Specifically, the optic nerve head has a well-defined collagenous lamina cribrosa (LC), spanning the scleral opening, with the axons of retinal ganglion cells organized into fascicles, beginning in the pre-laminar region, and becoming myelinated as they emerge from the distal side of the LC. We elaborate on these comparisons in the following discussion as the basis for arguing that the guinea pig is a potentially valuable model for investigating the association between myopia and glaucoma.

Our findings for the guinea pig optic nerve head contrast with the descriptions for the mice and rats of non-collagenous optic nerve heads. Interestingly, while all belong to the rodentia class, it has often been argued that the guinea pig is, in fact, not a rodent (D'Erchia et al., 1996; Frederiksen and Heeno Andersen, 2003; Graur et al., 1991), with some suggesting that the guinea pig may have diverged before the separation of the primates from other rodents (Graur et al., 1991). It has also been noted that the mitochondrial genome of the guinea pig contradicts rodent monophyly (D'Erchia et al., 1996).

In terms of biochemical composition and structural organization, the optic nerve head of the guinea pig bears closest resemblance to the optic nerve head of the tree shrew. For example, the collagenous beams of the guinea pig LC were found to be radially arranged, similar to the pattern described for the tree shrew (Albon et al., 2007), although qualitatively, the beams appear to be less dense in the guinea pig ONH (Albon et al., 2007). As in the tree shrew, the guinea pig LC contains collagen types I, III, IV and V, and the ONHs of both species include elastin and glial fibrillary acidic protein (GFAP). Elastin is commonly found in connective tissue, where it plays an important role in allowing tissue to return to their usual shape after stretching. In the ONH, elastin may help to minimize the stress generated by the deforming influence of IOP on axons passing through the LC. GFAP, an intermediate

filament protein, is a marker of glial cells. This protein is thought to contribute to the resilience and strength of astrocytes (Cullen et al., 2007), which have been shown to undergo reorientation in response to elevated IOP (Tehrani et al., 2014). It has thus been speculated that they play an important role in early glaucomatous optic nerve head changes. All of the above proteins have also been described in human ONHs (Albon et al., 1995; Hernandez et al., 1986; Morrison et al., 1989). These parallels are also important in the context of primary open angle glaucoma models; in humans, this disease causes elastin within the LC collagen beams to become disorganized and diminished (Quigley et al., 1991), and collagen type IV, normally localized to the septa, to extend into the nerve fiber bundles (Hernandez et al., 1990). While the magnification of antibody-labeled images in the current study (i.e., Figure 5) precluded localization of these various biochemical components, it was sufficient to confirm their presence in the optic nerve head.

In both humans and non-human primates, the collagen beams of the LC are surrounded by glial cells, forming channels that support the bundles of nerve fibers traversing the LC (Anderson, 1969; Furuta et al., 1993). H&E stained sections show numerous darkly stained nuclei outlining the surfaces of nerve fascicles, consistent with abundant GFAP labeling observed and thus a similar arrangement in the guinea pig ONH.

From SEM images, we were able to measure the dimensions of the scleral canal in a normal juvenile guinea pig; recorded diameters were also used to calculate a scleral canal area. However, these values are likely to underestimate *in vivo* dimensions, because of tissue shrinkage following fixation and dehydration, which may be as high as 20-30 percent (Johansson, 1987). Follow-up studies are warranted to characterize both changes in scleral canal size with age and with myopia, given that large ONHs, corresponding to large scleral canals, are known to be associated with early onset of glaucoma (Bellezza et al., 2003).

The LC is continuous with the sclera, which is intimately involved in myopic eye “growth” (enlargement), being the outer coat of the eye and ultimately the determinant of eye size (Rada et al., 2006). It thus seems plausible that the structure of the LC is also altered during myopic eye growth, and results from a number of different studies tend to be supportive of this idea. For example, like the LC, the parapapillary sclera of highly myopic human eyes is thinner than normal (Jonas et al., 2011) and the optic nerve heads of highly myopic eyes are reported to be different in appearance from those of eyes with lower myopia (Jonas et al., 1988; Xu et al., 2007a). In addition, longer eyes are associated with shallower LC depths, presumably due to changes in the scleral configuration with axial growth (Seo et al., 2014). It has been speculated that the posterior sclera exerts important biomechanical influences on the LC (Girard et al., 2009b; Norman et al.; Sigal et al.), and thus, it is of interest that in experimental myopia, increased eye elongation is associated with changes in both scleral composition (Gentle et al., 2003) and biomechanical properties (Siegwart and Norton, 1999). However, the LC has not been studied in a model of experimental myopia to-date.

One of the primary motivators for the current study was interest in finding a suitable animal model for studying the mechanism(s) underlying the apparent increased risk of primary open angle glaucoma in human myopes compared to non-myopes. The mouse, rat, rabbit and rhesus monkey are among the most widely used animal models of glaucoma and all have

also been used in experimental myopia studies, albeit only on a limited scale in the case of the rabbit and rat (Barathi et al., 2008; Pickett-Seltner et al., 1988; Smith et al., 1987; Tokoro, 1970). Because the LC has been implicated in glaucomatous nerve damage, an animal model that possesses a collagenous LC is most relevant. However, of the above-mentioned animal models of glaucoma, neither the mouse, nor rat nor rabbit possess a collagenous LC. Although glaucoma can be induced in chickens through exposure to constant light (Kinnear et al., 1974), the chicken has not been widely used in glaucoma research, despite its wide use in myopia research. The presence in the chicken of an ocular pecten, which precludes direct visibility of the optic nerve head *in vivo*, represents one obstacle to its adoption. Thus by a process of elimination alone, it can be argued that the guinea pig represents a most promising model for investigating the link between myopia and glaucoma. While yet to be tested directly, it is expected that methods used to increase IOP in other animal models, for example, the microbead method used in mice (Frankfort et al., 2013), and laser trabeculoplasty, as used in non-human primate (Ivers et al., 2015), can be adapted for use in guinea pigs.

The majority of experiments described here involved relatively young, 2-4 month-old guinea pigs. Nonetheless, guinea pigs are precocial animals, being well developed at birth, and reaching sexual maturity early, around 2 months of age. Studies have shown that visual function is also well developed by 2 months of age (Ostrin et al, 2011, IOVS E-Abstract 6296)(Huang et al., 1990). Thus it is likely that the ONH structural characteristics closely approximate those of healthy adult animals.

As a side note, it must be acknowledged that the guinea pig possesses a largely avascular retina. However, in terms of glaucoma, the vascularity of the ONH is likely of greater importance. In this context, blood vessels have been described in the laminar beams of the guinea pig ONH in a previous study (Furuta et al., 1993), and the fundus image captured for this study (i.e., Figure 2b), represents further supporting evidence that the ONH of the guinea pig is vascularized. In addition, the fundus image shows a barely visible cup. It is yet to be established whether the cup becomes more visible with axonal loss, as observed in humans. Nonetheless, OCT imaging of nerve fiber layer was shown to be feasible in the guinea pig (i.e., Figure 3), and potentially offers an important, additional method of following the course of glaucomatous changes as well as evaluating structural changes associated with myopic eye growth.

A suitable animal model for glaucoma requires that IOP can be measured in an efficient, reliable manner and that the range of normal IOPs are similar to those reported in humans, as they determine, at least in part, the stresses experienced by the retinal ganglion cell axons as they pass through the LC. Our study made use of the TonoLab, a rebound tonometer calibrated for the rat eye, whereas another study involving guinea pigs made use of the TonoVet, a rebound tonometer calibrated for much larger animal eyes, i.e., dog, cat and horse (Tao et al., 2013). In that study, absolute values were also not reported, IOP data being described only in terms of statistical significance of differences between treated and fellow control eyes for given conditions. Two other studies involving guinea pigs made use of applanation tonometers (Coster et al., 2008; Williams and Sullivan, 2010). In the first study using a Tonopen applanation tonometer to measure 100 normal guinea pigs (age unknown),

an average IOP of 16.5 ± 3.2 mmHg was reported (Williams and Sullivan, 2010), similar to the mean IOP of our 2 weeks-old animals (17.6 ± 2.6 mmHg), but significantly lower than our mean value for older animals (22.7 ± 2.3 mmHg). The other study using applanation tonometry reported a mean IOP of 18.27 ± 4.55 mmHg for 31 normal guinea pigs (age unknown)(Coster et al., 2008). In both of these studies, measurements were made in awake animals using a topical anesthetic. Note that while our study used a TonoLab, we found results to be no different from those collected with a Tonopen in a study of 30 guinea pig eyes (data not shown, $p = 0.87$). While manometric calibration for the guinea pig eyes is currently lacking for both instruments, the range of recorded IOP values are consistent with normal ranges reported for other animals. In our study, we also avoided the use of general anesthesia, after confirming in a pilot study that general anesthesia induced with ketamine/xylazine has a profound hypotensive effect, just as reported in other animals; measurements made on guinea pigs recovering from this anesthesia averaged 13.17 mmHg. Our choice of instrument had the added advantage of avoiding the need for topical corneal anesthesia.

In summary, this study showed that the ONH of guinea pig has a well-organized, collagen-based LC, similar in composition to that of humans. Thus, as a substitute for primate models, the guinea pig shows promise as a model for human ocular diseases that are known to affect the ONH, including myopia and glaucoma.

Acknowledgements

NIH NEI K08 EY022696 to LO and NIH NEI R01 EY012392 to CW, Thanks to Jessie Lee for assistance with TEM imaging

Abbreviations

POAG	primary open angle glaucoma
LC	lamina cribrosa
ONH	optic nerve head
RGC	retinal ganglion cell
IOP	intraocular pressure
SEM	scanning electron microscopy
TEM	transmission electron microscopy
OCT	optical coherence tomography

References

Albon J, Farrant S, Akhtar S, Young R, Boulton ME, Smith G, Taylor M, Guggenheim J, Morgan JE. Connective tissue structure of the tree shrew optic nerve and associated ageing changes. Invest Ophthalmol Vis Sci. 2007; 48:2134–2144. [PubMed: 17460272]

Albon J, Karwatowski WS, Avery N, Easty DL, Duance VC. Changes in the collagenous matrix of the aging human lamina cribrosa. Br J Ophthalmol. 1995; 79:368–375. [PubMed: 7742286]

Anderson DR. Ultrastructure of human and monkey lamina cribrosa and optic nerve head. Arch Ophthalmol. 1969; 82:800–814. [PubMed: 4982225]

Barathi VA, Boopathi VG, Yap EP, Beuerman RW. Two models of experimental myopia in the mouse. Vision Res. 2008; 48:904–916. [PubMed: 18289630]

Bellezza AJ, Rintalan CJ, Thompson HW, Downs JC, Hart RT, Burgoyne CF. Deformation of the lamina cribrosa and anterior scleral canal wall in early experimental glaucoma. Invest Ophthalmol Vis Sci. 2003; 44:623–637. [PubMed: 12556392]

Brooks DE, Arellano E, Kubilis PS, Komaromy AM. Histomorphometry of the porcine scleral lamina cribrosa surface. Veterinary ophthalmology. 1998; 1:129–135. [PubMed: 11397222]

Brooks DE, Samuelson DA, Gelatt KN, Smith PJ. Morphologic changes in the lamina cribrosa of beagles with primary open-angle glaucoma. American journal of veterinary research. 1989; 50:936–941. [PubMed: 2764346]

Burgoyne CF, Downs JC, Bellezza AJ, Suh JK, Hart RT. The optic nerve head as a biomechanical structure: a new paradigm for understanding the role of IOP-related stress and strain in the pathophysiology of glaucomatous optic nerve head damage. Prog Retin Eye Res. 2005; 24:39–73. [PubMed: 15555526]

Casson RJ, Gupta A, Newland HS, McGovern S, Muecke J, Selva D, Aung T. Risk factors for primary open-angle glaucoma in a Burmese population: the Meiktila Eye Study. Clin Experiment Ophthalmol. 2007; 35:739–744. [PubMed: 17997778]

Coster ME, Stiles J, Krohne SG, Raskin RE. Results of diagnostic ophthalmic testing in healthy guinea pigs. Journal of the American Veterinary Medical Association. 2008; 232:1825–1833. [PubMed: 18598151]

Cullen DK, Simon CM, LaPlaca MC. Strain rate-dependent induction of reactive astrogliosis and cell death in three-dimensional neuronal-astrocytic co-cultures. Brain Res. 2007; 1158:103–115. [PubMed: 17555726]

D'Erchia AM, Gissi C, Pesole G, Saccone C, Arnason U. The guinea-pig is not a rodent. Nature. 1996; 381:597–600. [PubMed: 8637593]

Faulkner AE, Kim MK, Iuvone PM, Pardue MT. Head-mounted goggles for murine form deprivation myopia. J Neurosci Methods. 2007; 161:96–100. [PubMed: 17126909]

Flitcroft DI. The complex interactions of retinal, optical and environmental factors in myopia aetiology. Prog Retin Eye Res. 2012; 31:622–660. [PubMed: 22772022]

Fong DS, Epstein DL, Allingham RR. Glaucoma and myopia: are they related? Int Ophthalmol Clin. 1990; 30:215–218. [PubMed: 2199391]

Frankfort BJ, Khan AK, Tse DY, Chung I, Pang JJ, Yang Z, Gross RL, Wu SM. Elevated intraocular pressure causes inner retinal dysfunction before cell loss in a mouse model of experimental glaucoma. Invest Ophthalmol Vis Sci. 2013; 54:762–770. [PubMed: 23221072]

Frederiksen S, Heeno Andersen J. The external promoter in the guinea pig 5S rRNA gene is different from the rodent promoter. Hereditas. 2003; 139:156–160. [PubMed: 15061817]

Fujita Y, Imagawa T, Uehara M. Comparative study of the lamina cribrosa and the pial septa in the vertebrate optic nerve and their relationship to the myelinated axons. Tissue & cell. 2000; 32:293–301. [PubMed: 11145012]

Furuta M, Lindsey JD, Weinreb RN. Ultrastructure of glial cells and extracellular matrix in the Guinea pig lamina cribrosa. J Glaucoma. 1993; 2:303–312. [PubMed: 19920537]

Gaasterland D, Kupfer C. Experimental glaucoma in the rhesus monkey. Invest Ophthalmol. 1974; 13:455–457. [PubMed: 4208801]

Gentle A, Liu Y, Martin JE, Conti GL, McBrien NA. Collagen gene expression and the altered accumulation of scleral collagen during the development of high myopia. J Biol Chem. 2003; 278:16587–16594. [PubMed: 12606541]

Girard MJ, Downs JC, Bottlang M, Burgoyne CF, Suh JK. Peripapillary and posterior scleral mechanics--part II: experimental and inverse finite element characterization. J Biomech Eng. 2009a; 131:051012. [PubMed: 19388782]

Girard MJ, Downs JC, Burgoyne CF, Suh JK. Peripapillary and posterior scleral mechanics--part I: development of an anisotropic hyperelastic constitutive model. J Biomech Eng. 2009b; 131:051011. [PubMed: 19388781]

Graur D, Hide WA, Li WH. Is the guinea-pig a rodent? Nature. 1991; 351:649–652. [PubMed: 2052090]

Gross RL, Ji J, Chang P, Pennesi ME, Yang Z, Zhang J, Wu SM. A mouse model of elevated intraocular pressure: retina and optic nerve findings. Trans Am Ophthalmol Soc. 2003; 101:163–169. discussion 169-171. [PubMed: 14971574]

Hayreh SS. Blood supply of the optic nerve head and its role in optic atrophy, glaucoma, and oedema of the optic disc. Br J Ophthalmol. 1969; 53:721–748. [PubMed: 4982590]

Hernandez MR, Andrzejewska WM, Neufeld AH. Changes in the extracellular matrix of the human optic nerve head in primary open-angle glaucoma. Am J Ophthalmol. 1990; 109:180–188. [PubMed: 2405683]

Hernandez MR, Igoe F, Neufeld AH. Extracellular matrix of the human optic nerve head. Am J Ophthalmol. 1986; 102:139–148. [PubMed: 2426947]

Howlett MH, McFadden SA. Form-deprivation myopia in the guinea pig (Cavia porcellus). Vision Res. 2006; 46:267–283. [PubMed: 16139323]

Howlett MH, McFadden SA. Spectacle lens compensation in the pigmented guinea pig. Vision Res. 2009; 49:219–227. [PubMed: 18992765]

Huang J, Wyse JP, Spira AW. Ontogenesis of the electroretinogram in a precocial mammal, the guinea pig (Cavia porcellus). Comp Biochem Physiol A Comp Physiol. 1990; 95:149–155. [PubMed: 1968807]

Hung KH, Cheng CY, Liu CJ. Risk factors for predicting visual field progression in Chinese patients with primary open-angle glaucoma: A retrospective study. J Chin Med Assoc. 2015; 78:418–423. [PubMed: 25819708]

Ivers KM, Sredar N, Patel NB, Rajagopalan L, Queener HM, Twa MD, Harwerth RS, Porter J. In Vivo Changes in Lamina Cribrosa Microarchitecture and Optic Nerve Head Structure in Early Experimental Glaucoma. PloS one. 2015; 10:e0134223. [PubMed: 26230993]

Jiang L, Long K, Schaeffel F, Zhou X, Zheng Y, Ying H, Lu F, Stell WK, Qu J. Effects of dopaminergic agents on progression of naturally occurring myopia in albino guinea pigs (Cavia porcellus). Invest Ophthalmol Vis Sci. 2014; 55:7508–7519. [PubMed: 25270191]

Johansson JO. The lamina cribrosa in the eyes of rats, hamsters, gerbils and guinea pigs. Acta anatomica. 1987; 128:55–62. [PubMed: 3825488]

Jonas JB, Berenshtein E, Holbach L. Lamina cribrosa thickness and spatial relationships between intraocular space and cerebrospinal fluid space in highly myopic eyes. Invest Ophthalmol Vis Sci. 2004; 45:2660–2665. [PubMed: 15277489]

Jonas JB, Budde WM. Optic nerve damage in highly myopic eyes with chronic open-angle glaucoma. Eur J Ophthalmol. 2005; 15:41–47. [PubMed: 15751238]

Jonas JB, Gusek GC, Naumann GO. Optic disk morphometry in high myopia. Graefes Arch Clin Exp Ophthalmol. 1988; 226:587–590. [PubMed: 3209086]

Jonas JB, Jonas SB, Jonas RA, Holbach L, Panda-Jonas S. Histology of the parapapillary region in high myopia. Am J Ophthalmol. 2011; 152:1021–1029. [PubMed: 21821229]

Jonas JB, Mardin CY, Schlotzer-Schrehardt U, Naumann GO. Morphometry of the human lamina cribrosa surface. Invest Ophthalmol Vis Sci. 1991; 32:401–405. [PubMed: 1993592]

Kinnear A, Lauber JK, Boyd TA. Genesis of light-induced avian glaucoma. Invest Ophthalmol. 1974; 13:872–875. [PubMed: 4431488]

Liang YB, Friedman DS, Zhou Q, Yang X, Sun LP, Guo LX, Tao QS, Chang DS, Wang NL. Prevalence of Primary Open Angle Glaucoma in a Rural Adult Chinese Population: The Handan Eye Study. Invest Ophthalmol Vis Sci.

May CA, Lutjen-Drecoll E. Morphology of the murine optic nerve. Invest Ophthalmol Vis Sci. 2002; 43:2206–2212. [PubMed: 12091418]

Miki A, Ikuno Y, Asai T, Usui S, Nishida K. Defects of the Lamina Cribrosa in High Myopia and Glaucoma. PloS one. 2015; 10:e0137909. [PubMed: 26366870]

Mitchell P, Hourihan F, Sandbach J, Wang JJ. The relationship between glaucoma and myopia: the Blue Mountains Eye Study. Ophthalmology. 1999; 106:2010–2015. [PubMed: 10519600]

Morcos Y, Chan-Ling T. Concentration of astrocytic filaments at the retinal optic nerve junction is coincident with the absence of intra-retinal myelination: comparative and developmental evidence. Journal of neurocytology. 2000; 29:665–678. [PubMed: 11353290]

Morrison JC, Dorman-Pease ME, Dunkelberger GR, Quigley HA. Optic nerve head extracellular matrix in primary optic atrophy and experimental glaucoma. Arch Ophthalmol. 1990; 108:1020–1024. [PubMed: 2369339]

Morrison JC, Jerdan JA, Dorman ME, Quigley HA. Structural proteins of the neonatal and adult lamina cribrosa. Arch Ophthalmol. 1989; 107:1220–1224. [PubMed: 2757553]

Norman RE, Flanagan JG, Sigal IA, Rausch SM, Tertinegg I, Ethier CR. Finite element modeling of the human sclera: influence on optic nerve head biomechanics and connections with glaucoma. Exp Eye Res. 93:4–12. [PubMed: 20883693]

Pan CW, Cheung CY, Aung T, Cheung CM, Zheng YF, Wu RY, Mitchell P, Lavanya R, Baskaran M, Wang JJ, Wong TY, Saw SM. Differential associations of myopia with major age-related eye diseases: the Singapore Indian Eye Study. Ophthalmology. 2013; 120:284–291. [PubMed: 23084122]

Pascolini D, Mariotti SP. Global estimates of visual impairment: 2010. Br J Ophthalmol. 2012; 96:614–618. [PubMed: 22133988]

Perdicchi A, Iester M, Scuderi G, Amodeo S, Medori EM, Recupero SM. Visual field damage and progression in glaucomatous myopic eyes. Eur J Ophthalmol. 2007; 17:534–537. [PubMed: 17671927]

Pickett-Seltner RL, Sivak JG, Pasternak JJ. Experimentally induced myopia in chicks: morphometric and biochemical analysis during the first 14 days after hatching. Vision Res. 1988; 28:323–328. [PubMed: 3414019]

Pierro L, Camesasca FI, Mischi M, Brancato R. Peripheral retinal changes and axial myopia. Retina. 1992; 12:12–17. [PubMed: 1565864]

Pucker AD, Carpenter AR, McHugh KM, Mutti DO. Guinea pig ciliary muscle development. Optom Vis Sci. 2014; 91:730–739. [PubMed: 24901488]

Quigley HA, Brown A, Dorman-Pease ME. Alterations in elastin of the optic nerve head in human and experimental glaucoma. Br J Ophthalmol. 1991; 75:552–557. [PubMed: 1911659]

Quigley HA, Guy J, Anderson DR. Blockade of rapid axonal transport. Effect of intraocular pressure elevation in primate optic nerve. Arch Ophthalmol. 1979; 97:525–531. [PubMed: 84662]

Quigley HA, Hohman RM, Addicks EM, Massof RW, Green WR. Morphologic changes in the lamina cribrosa correlated with neural loss in open-angle glaucoma. Am J Ophthalmol. 1983; 95:673–691. [PubMed: 6846459]

Rada JA, Shelton S, Norton TT. The sclera and myopia. Exp Eye Res. 2006; 82:185–200. [PubMed: 16202407]

Radius RL, Bade B. The anatomy at the lamina cribrosa in the normal cat eye. Arch Ophthalmol. 1982; 100:1658–1660. [PubMed: 7138335]

Roberts MD, Grau V, Grimm J, Reynaud J, Bellezza AJ, Burgoyne CF, Downs JC. Remodeling of the connective tissue microarchitecture of the lamina cribrosa in early experimental glaucoma. Invest Ophthalmol Vis Sci. 2009; 50:681–690. [PubMed: 18806292]

Rodriguez-Ramos Fernandez J, Dubielzig RR. Ocular comparative anatomy of the family Rodentia. Veterinary ophthalmology. 2013; 16(Suppl 1):94–99. [PubMed: 23734597]

Scott R, Grosvenor T. Structural model for emmetropic and myopic eyes. Ophthalmic Physiol Opt. 1993; 13:41–47. [PubMed: 8510947]

Seo JH, Kim TW, Weinreb RN. Lamina cribrosa depth in healthy eyes. Invest Ophthalmol Vis Sci. 2014; 55:1241–1251. [PubMed: 24474269]

Siegwart JT Jr. Norton TT. Regulation of the mechanical properties of tree shrew sclera by the visual environment. Vision Res. 1999; 39:387–407. [PubMed: 10326144]

Sigal IA, Yang H, Roberts MD, Burgoyne CF, Downs JC. IOP-induced lamina cribrosa displacement and scleral canal expansion: an analysis of factor interactions using parameterized eye-specific models. Invest Ophthalmol Vis Sci. 52:1896–1907. [PubMed: 20881292]

Sigal IA, Yang H, Roberts MD, Grimm JL, Burgoyne CF, Demirel S, Downs JC. IOP-induced lamina cribrosa deformation and scleral canal expansion: independent or related? Invest Ophthalmol Vis Sci. 2011; 52:9023–9032. [PubMed: 21989723]

Smith EL 3rd, Harwerth RS, Crawford ML, von Noorden GK. Observations on the effects of form deprivation on the refractive status of the monkey. Invest Ophthalmol Vis Sci. 1987; 28:1236–1245. [PubMed: 3610541]

Sohn SW, Song JS, Kee C. Influence of the extent of myopia on the progression of normal-tension glaucoma. Am J Ophthalmol. 2010; 149:831–838. [PubMed: 20231010]

Sossi N, Anderson DR. Blockage of axonal transport in optic nerve induced by elevation of intraocular pressure. Effect of arterial hypertension induced by angiotensin I. Arch Ophthalmol. 1983; 101:94–97. [PubMed: 6185108]

Tao Y, Pan M, Liu S, Fang F, Lu R, Lu C, Zheng M, An J, Xu H, Zhao F, Chen JF, Qu J, Zhou X. cAMP level modulates scleral collagen remodeling, a critical step in the development of myopia. PloS one. 2013; 8:e71441. [PubMed: 23951163]

Tehrani S, Johnson EC, Cepurna WO, Morrison JC. Astrocyte processes label for filamentous actin and reorient early within the optic nerve head in a rat glaucoma model. Invest Ophthalmol Vis Sci. 2014; 55:6945–6952. [PubMed: 25257054]

Tokoro T. Experimental myopia in rabbits. Invest Ophthalmol. 1970; 9:926–934. [PubMed: 5484804]

Troilo D, Gottlieb MD, Wallman J. Visual deprivation causes myopia in chicks with optic nerve section. Curr Eye Res. 1987; 6:993–999. [PubMed: 3665562]

Vilupuru AS, Rangaswamy NV, Frishman LJ, Smith EL 3rd, Harwerth RS, Roorda A. Adaptive optics scanning laser ophthalmoscopy for in vivo imaging of lamina cribrosa. J Opt Soc Am A Opt Image Sci Vis. 2007; 24:1417–1425. [PubMed: 17429488]

Vitale S, Sperduto RD, Ferris FL 3rd. Increased prevalence of myopia in the United States between 1971-1972 and 1999-2004. Arch Ophthalmol. 2009; 127:1632–1639. [PubMed: 20008719]

Wallman J, Gottlieb MD, Rajaram V, Fugate-Wentzek LA. Local retinal regions control local eye growth and myopia. Science. 1987; 237:73–77. [PubMed: 3603011]

Wang JY, Liu SZ, Wei X, Wu XY, Tan XP. [High myopia and retinal ultrastructure of albino guinea-pigs]. Zhong nan da xue xue bao. Yi xue ban = Journal of Central South University. Medical sciences. 2007; 32:282–287. [PubMed: 17478937]

Williams D, Sullivan A. Ocular disease in the guinea pig (Cavia porcellus): a survey of 1000 animals. Veterinary ophthalmology. 2010; 13(Suppl):54–62. [PubMed: 20840091]

Wong TY, Klein BE, Klein R, Knudtson M, Lee KE. Refractive errors, intraocular pressure, and glaucoma in a white population. Ophthalmology. 2003; 110:211–217. [PubMed: 12511368]

Xu L, Li Y, Wang S, Wang Y, Jonas JB. Characteristics of highly myopic eyes: the Beijing Eye Study. Ophthalmology. 2007a; 114:121–126. [PubMed: 17070594]

Xu L, Wang Y, Wang S, Jonas JB. High myopia and glaucoma susceptibility the Beijing Eye Study. Ophthalmology. 2007b; 114:216–220. [PubMed: 17123613]

Yang H, Downs JC, Girkin C, Sakata L, Bellezza A, Thompson H, Burgoyne CF. 3-D histomorphometry of the normal and early glaucomatous monkey optic nerve head: lamina cribrosa and peripapillary scleral position and thickness. Invest Ophthalmol Vis Sci. 2007; 48:4597–4607. [PubMed: 17898283]

Highlights

- The guinea pig possesses a radially oriented collagenous lamina cribrosa
- Protein content of the guinea pig lamina cribrosa is similar to humans and non-human primates
- Intraocular pressure in the guinea pig is readily measured in awake animals and ranges from 17.3-22.7 mmHg, undergoing a diurnal fluctuation that peaks in the morning.
- The guinea pig represents a promising model for human ocular disease including myopia and glaucoma

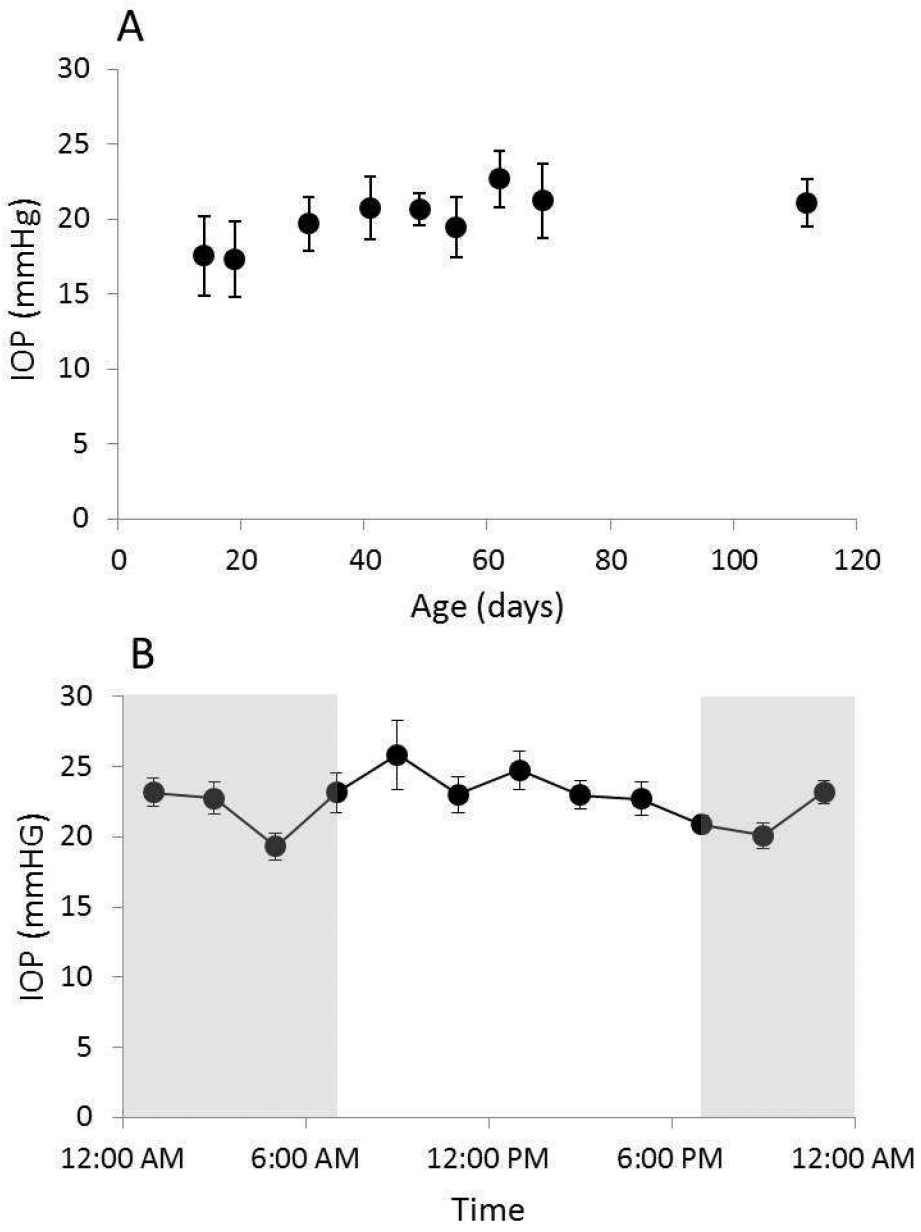

Figure 1.

A) Mean IOP (± SE) of right eyes, recorded over a 3-month period from pigmented guinea pigs (n = 6), starting at 2 weeks of age. B) Mean IOP (± SE) of right eyes measured at 2 hour intervals over a 24 hour period (n = 12), gray area represents the dark phase

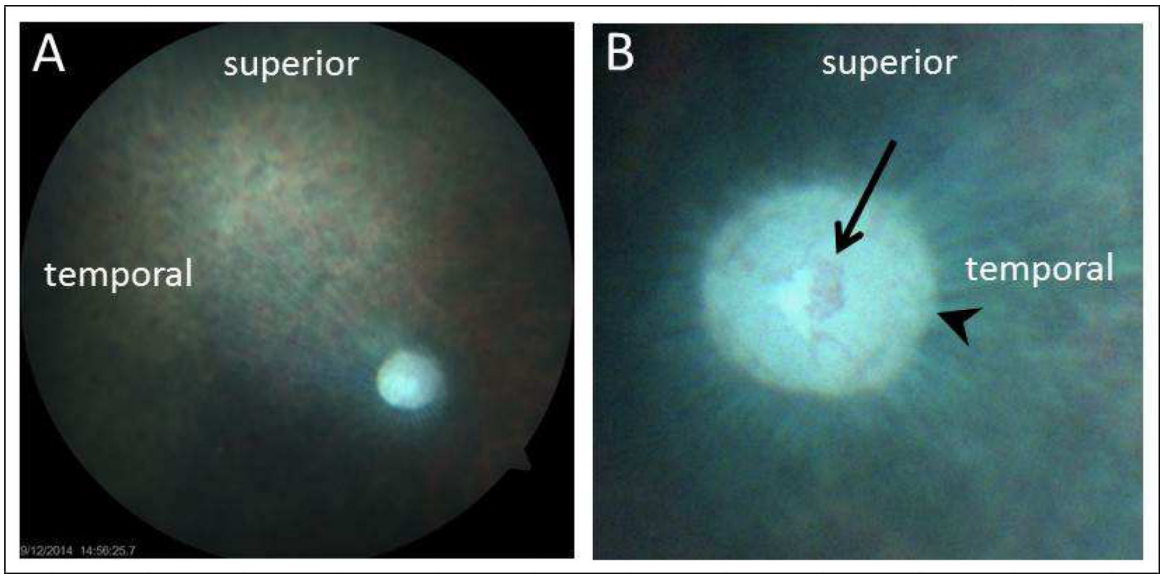

Figure 2.

Representative fundus photos taken from a 4 month-old pigmented guinea pig; A) low magnification, 30° field of the right eye; B) higher magnification, 15° field centered on optic nerve head of the left eye. The principal fundus landmark is the optic nerve head, which has a well define rim (arrowhead) and a central concentration of blood vessels (arrow); the retina is otherwise largely avascular.

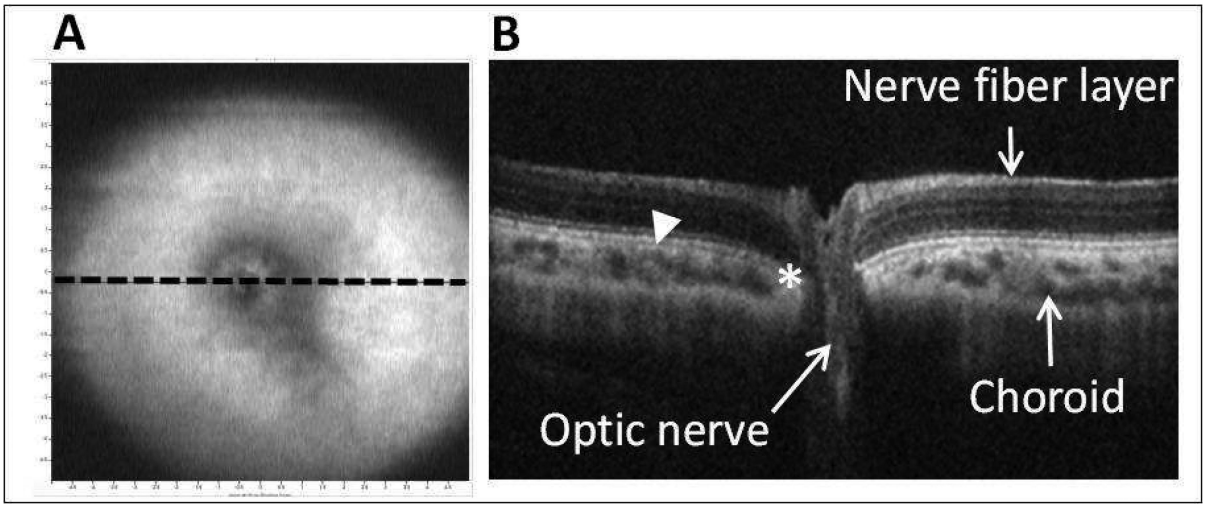

Figure 3.

In vivo SD-OCT images from a 2 month-old pigmented guinea pig: A) low resolution en face volume intensity projection, indicating location of cross-sectional image in B (dotted line); and B) corresponding OCT image through optic nerve head (14 mm line scan, arrowhead: chorioretinal border; asterisk: termination of Bruch's membrane).

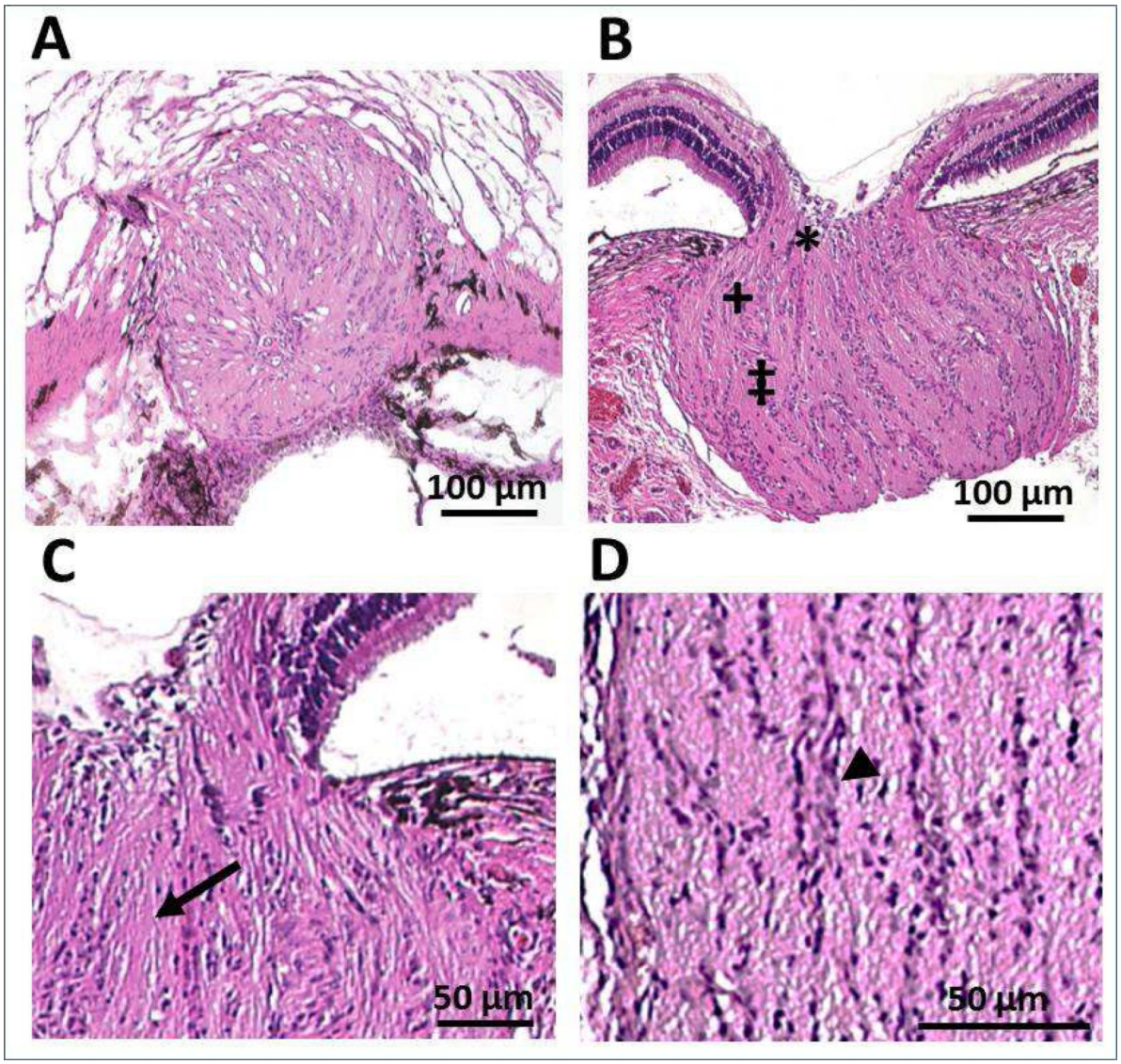

Figure 4.

H & E stained sections of the optic nerve head of a 9 weeks-old pigmented guinea pig; low magnification A) en face view at the level of the lamina cribrosa, cut at a slight angle with visible sclera superiorly and retina inferiorly, and B) cross-sectional view, including pre-laminar (*), laminar (+) and post-laminar regions (‡). Laminar region represents the section shown in (A); high magnification cross sectional views of C) pre-laminar and laminar regions (arrow: nerve fiber bundles) and D) the post-laminar region (arrowhead: presumed glial cells). Scale bars represent 100 µm (A & B) and 50 µm (C & D).

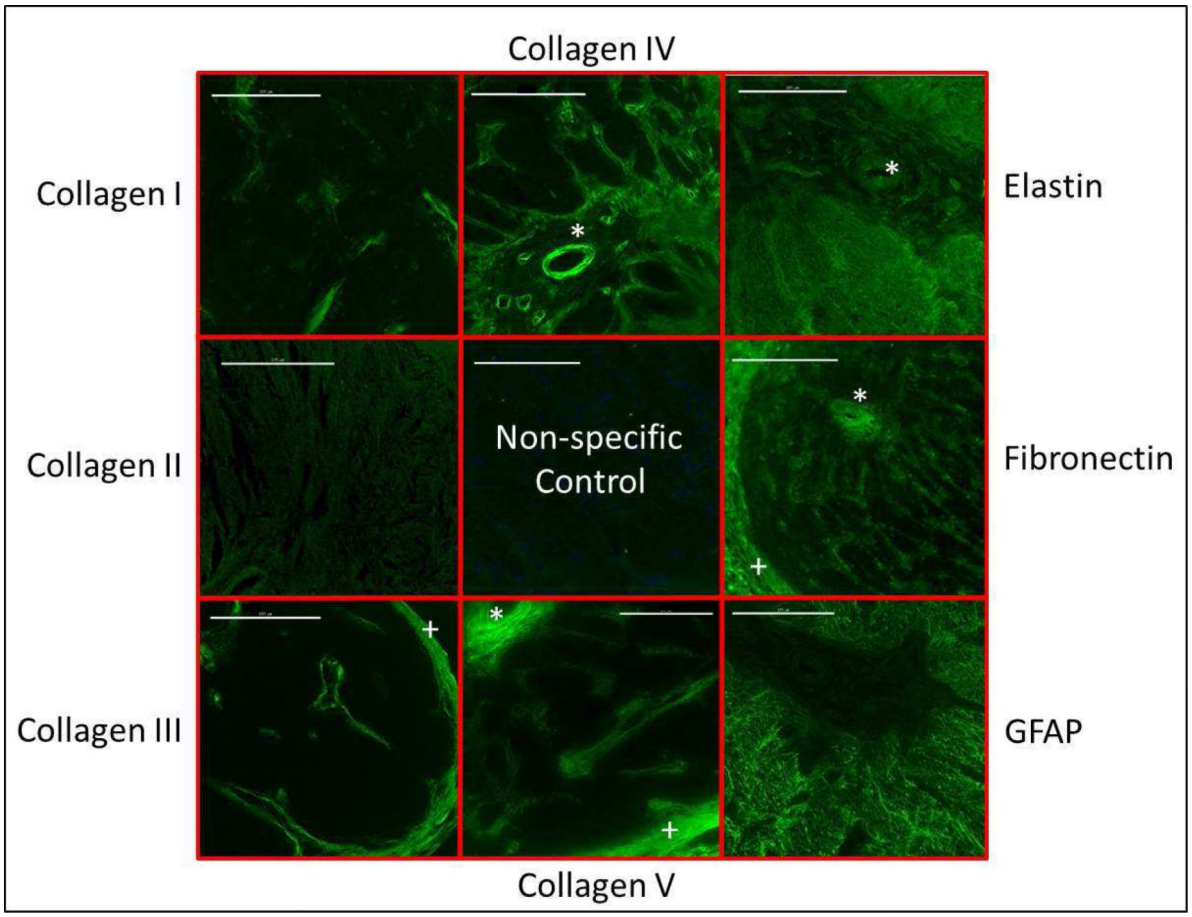

Figure 5.

Immunostained sections of the optic nerve head of a pigmented guinea pig, taken at the level of the lamina, showing the presence of collagen types I, III IV and V, as well as elastin, fibronectin and GFAP. Collagen II was not found in this region. Scale bar represent 100 μm. * vascular sheath; + surrounding meninges

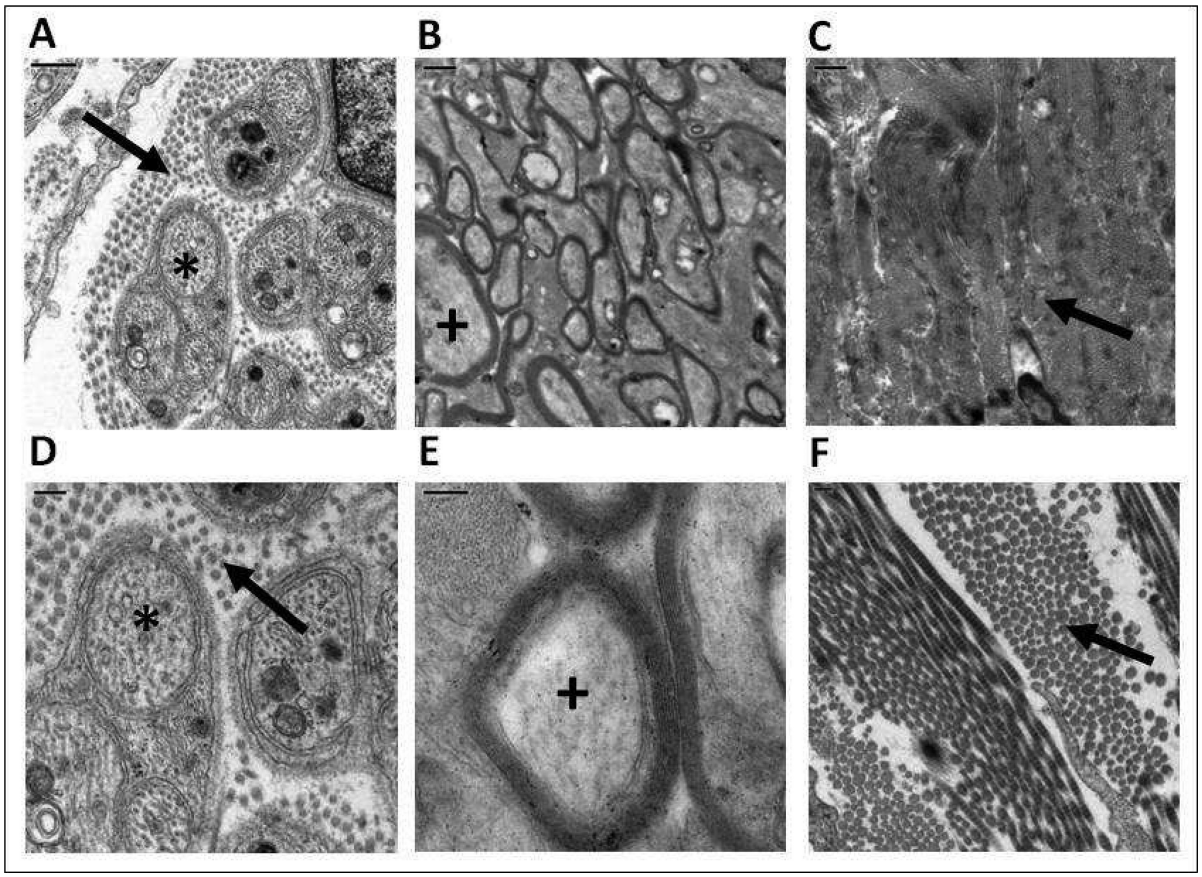

Figure 6.

TEM images of the optic nerve from the pre-laminar region (A & D; scale bars represent 0.5 & 0.2 μm respectively), and post-laminar region (B & E; scale bars represent 1 & 0.2 μm, respectively), as well as peripapillary sclera (C & F; scale bars represent 1 & 0.2 μm, respectively); * non-myelinated nerve fiber bundles; + myelinated nerve bundles; arrows identify collagen fibrils.

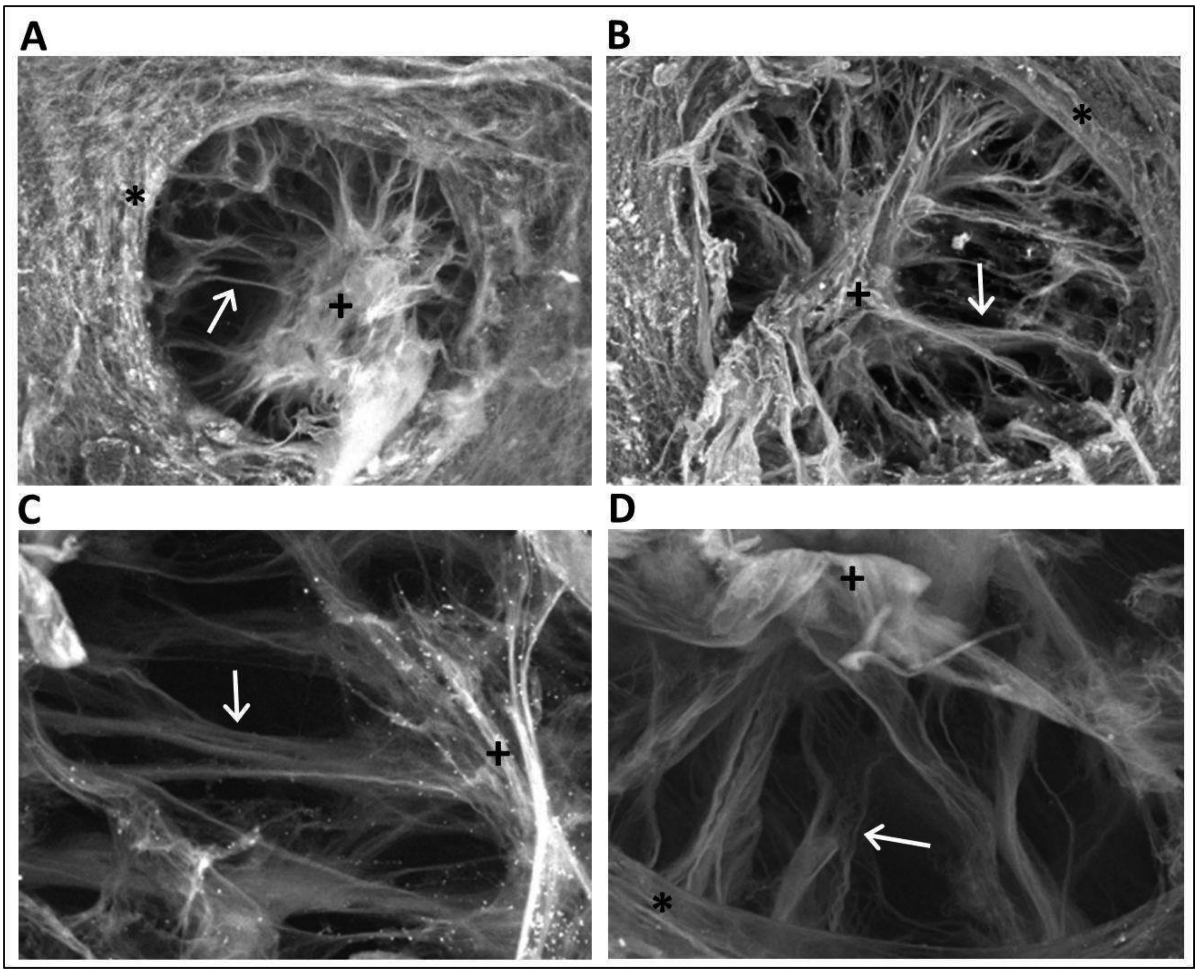

Figure 7.

Representative images of optic nerve heads subjected to alkali maceration and subsequent processing for SEM, from the eyes of a 4 months-old pigmented guinea pig (A & C) and an older (>1 year) albino guinea pig (B & D). Arrows identify laminar beams, + vascular sheath, * peripapillary sclera; Scale bars represent 200 μm (A & B) and 50 μm (C & D).

Table 1

Summary of findings from various studies characterizing the structure of the lamina cribrosa (LC) in various species.

Investigators	Species	Lamina Cribrosa
(May and Lutjen-Drecoll, 2002)	Lab mouse	non-collagenous
(Rodriguez-Ramos Fernandez and Dubielzig, 2013)	deer mouse, Norway rat, dwarf hamster, meadow vole	
(Morcos and Chan-Ling, 2000)	rabbit, quail, chicken	
(Johansson, 1987)	hamster, pvg hooded rat	simple collagenous
(Rodriguez-Ramos Fernandez and Dubielzig, 2013)	porcupine, capybara, flying squirrel, western gray squirrel	
(Johansson, 1987),	gerbil, guinea pig	well developed collagenous
(Morcos and Chan-Ling, 2000)	marmoset, flying fox, cat, sheep	
(Albon et al., 2007)	tree shrew	
(Brooks et al., 1998)	pig	
(Brooks et al., 1989)	dog	
(Radius and Bade, 1982)	cat	
(Vilupuru et al., 2007)	rhesus monkey	
(Jonas et al., 1991)	human	

Table 2

Number, type and age of guinea pigs used in each component of this study.

Procedures & measurements	Number & type of guinea pig (age)
IOP (development)	6 pigmented (2-20 weeks)
IOP (circadian)	12 pigmented (12-18 months)
Fundus photography	1 pigmented (4 months)
OCT imaging	1 pigmented (2 months)
Histology: Immunostaining	3 pigmented (2 months)
Histology: H& E staining	1 pigmented (2 months)
TEM	1 pigmented (2 months) 1 albino (2 months)
SEM	2pigmented (2 months) 3albino (2 months)